Thermal Elevation in the Human Eye and Head Due to the Operation of a Retinal Prosthesis

Keyoor Gosalia, *Student Member, IEEE*, James Weiland, *Member, IEEE*, Mark Humayun, *Member, IEEE*, and Gianluca Lazzi*, *Senior Member, IEEE*

***Abstract*—An explicit finite-difference time-domain formulation of the bio-heat equation is employed with a three-dimensional head eye model to evaluate the temperature increase in the eye and surrounding head tissues due to the operation of the implanted stimulator IC chip of a retinal prosthesis designed to restore partial vision to the blind. As a first step, a validation of the thermal model and method used is carried out by comparison with *in vivo* measurements of intraocular heating performed in the eyes of dogs. Induced temperature increase in the eye and surrounding tissues is then estimated for several different operational conditions of the implanted chip. In the vitreous cavity, temperature elevation of 0.26 °C is observed after 26 min for a chip dissipating 12.4 mW when positioned in the mid-vitreous cavity while it is 0.16 °C when the chip is positioned in the anterior portion between the eye's ciliary muscles. Corresponding temperature rises observed on chip are 0.82 °C for both the positions of the chip. A comprehensive account of temperature elevations in different tissues under different operational conditions is presented.**

***Index Terms*—Bio-heat equation, dosimetry, retinal prosthesis, thermal elevation.**

I. Introduction

In a healthy retina, photoreceptor cells (rods/cones) initiate a neural signal in response to light. Progressive loss of photoreceptors of the retina leads to diseases like retinitis pigmentosa (RP) and age-related macular degeneration (AMD) causing blindness in over 10 million people worldwide. In end-stage RP and AMD patients, photoreceptors are almost completely defective but the cells to which they synapse with-the bipolar and ganglion cells-may survive at higher rates [1]. Clinically, it has been demonstrated that artificial electrical stimulation of the surviving ganglion cells can elicit visual perception in patients [2], [3].

Hence, a rehabilitative prosthetic device can be designed to provide artificial pattern electrical stimulation on the retina and thus partially reverse the visual loss [4]. Currently, several efforts are underway to design such a retinal prosthesis [5]–[8]. One of the proposed systems consists of an extraocular and an intraocular unit [5]. The extraocular unit includes a camera for image collection, data encoding chip and a primary coil for inductive power and data communication. A secondary coil, signal processing chips, current stimulator chip and an electrode array make up the intraocular unit [9], [10].

Operation of the power and data communication (wireless telemetry) link leads to electromagnetic (EM) power absorption in the eye and surrounding tissues and the physiological hazards due to EM power deposition in tissues are known to be largely thermal in nature [11]. Also, the power dissipation due to operation of the implanted chip leads to increase in the natural steady-state temperature of the eye and surrounding head tissues. Hence, both the deposited EM energy due to wireless telemetry link (quantified in terms of specific absorption rate or SAR) as well as the power dissipation in the implanted electronics account for the heating induced in the eye and head tissues [12].

Several studies have been conducted to investigate the temperature increase in head and eye due to cell phone usage [13], [14] in the presence of wireless LANs [15] or to determine heating induced in the eye and formation of cataracts [16]–[18]. In [12], SAR and thermal elevation in a two-dimensional (2-D) model of the human head and eye due to the operation of the retinal prosthesis is computed. As is mentioned in [12], a three-dimensional (3-D) model is essential for a complete characterization of the temperature distribution in implanted electronics and to model the heat flow in the head. In this paper, first we present the methods and models employed to compute thermal elevation in a 3-D human head-eye model due to the operation of the wireless telemetry link and implanted electronics of a retinal prosthesis. Finally, we present the computed temperature rise in the various tissues of the head model.

This paper is organized into six main sections. A description of the anatomically accurate head model (and its portions) used in the computational domain is given in Section II followed by a brief summary of the numerical methods employed in Section III. Section IV shows a validation of the thermal model used in simulations by comparison with measured data obtained from experiments involving implanted heaters in the eyes of dogs. Simulated results on power absorption due to operation of the wireless link and temperature increase in the head model due to the implanted chip power dissipation are reported in Section V. Influence of different positions, orientations, sizes, and power dissipation levels of the implanted chip on thermal elevation are investigated. Finally, Section VI concludes with a summary of results and insights gained into the thermal effects due to the operation of a retinal prosthesis.

Manuscript received August 25, 2003; revised December 1, 2003. This work was supported in part by the Whitaker Foundation under Contract RG-00-0298, in part by the National Science Foundation (NSF) under CAREER award ECS-0091599, in part by the Office of Science (BER), U.S. Department of Energy, under Grant DE-FG02-04ER63752, and in part by the NSF under Grant EEC-0310723. *Asterisk indicates corresponding author.*

K. Gosalia is with the North Carolina State University, Raleigh, NC 27695-7914 USA.

J. Weiland and M. Humayun are with the Doheny Retina Institute, Keck School of Medicine, University of Southern California, Los Angeles, CA 90007 USA.

*G. Lazzi is with the North Carolina State University, Raleigh, NC 27695-7914, USA (e-mail: lazzi@eos.ncsu.edu).

Digital Object Identifier 10.1109/TBME.2004.827548

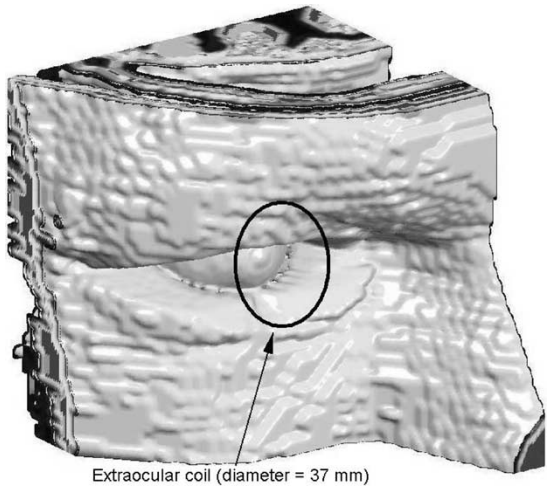

Fig. 1. Head model utilized for computing the SAR induced due to wireless telemetry link.

II. Human Head Model

The data for the head model was obtained in the form of cross sectional slices of 1 mm resolution from the National Library of Medicine (NLM) "Visible Man Project" [19]. In this application, since it was essential to represent the tissues of the eye and head with a high degree of detail, the head model was discretized further-to reach a spatial resolution of 0.25 mm (64 times the original one) using a method of interpolation in all three dimensions [20]. The detailed features of the eye were represented as described in [12] and the dielectric properties of the body tissues at the frequency of 10 MHz were obtained from the online database compiled by Gabriel [21]. For the SAR computation, a portion of this head model was extracted and used in the computational domain, as shown in Fig. 1.

While computing the initial basal temperature distribution, almost the whole upper portion of the head was included in the computational domain as shown in Fig. 2. This was done to ensure that the inaccuracies in the temperature distribution due to the abrupt truncation of the head model occurred at regions far removed from the eye and its surrounding head tissues. A portion of the head model similar to the one shown in Fig. 1 was extracted and utilized in the computational domain for thermal elevation computations. The resolution of the model was reduced to 0.5 mm to reduce the size of the model and hence save on the computational resources of time and memory.

The eye lens was removed in all cases of SAR computations and simulations for thermal elevations since the intraocular unit of the retinal prosthesis is meant to be encapsulated and hinged in between the eye's ciliary muscle.

III. Methods for Computational Analysis

EM energy is deposited in the eye and surrounding head tissues due to the operation of the wireless telemetry link-inductive power and data transfer through coils at a low frequency (2–10 MHz). The finite-difference time-domain (FDTD) method is employed to quantify the power deposition in terms of SAR and, depending on whether the SAR values are within the stipulated guidelines [22], they are included along with the power dissipation of the chip in the eye as the external sources of thermal elevation in the thermal simulations.

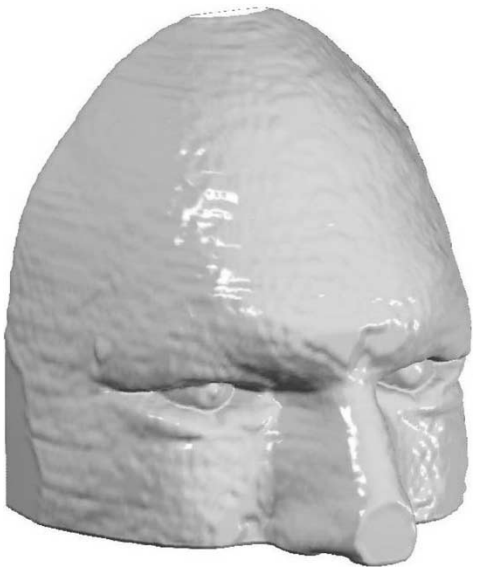

Fig. 2. Head model utilized for computing the initial steady-state temperature distribution.

A. SAR Computation

A 3-D D-H formulation of the FDTD method [23] is used to compute the induced EM energy in a 0.25-mm resolution head model. Material independent perfectly matched layer (PML) is used as an absorbing boundary condition so that the model can be immersed in the PML layers as mentioned in [24].

For computing the SAR induced by the wireless telemetry link, a circular coil of approximately 37-mm diameter is modeled at a distance of 20 mm from the eye and excited by a 2-A current at 10 MHz. Absorbed power is quantified as $\mathrm{SAR} = \sigma|\vec{E}|^2/2\rho$ in [W/kg] for conductivity, σ, electric field $\vec{E}$, and mass density, ρ at each cell. In order to determine their conformity to the IEEE/ANSI standard [22], peak 1-g SAR (SAR_{1g}) are evaluated.

B. Thermal Model

Thermal elevation in biological tissue can be computed by means of the bio-heat equation. The formulation of the bio-heat equation for numerical implementation in this work closely parallels that in [12], [25], and will only be briefly summarized here. Taking into account external thermal sources, the bio-heat equation can be written as

$$C\rho\frac{\partial T}{\partial t} = \nabla\cdot(K\nabla T) + A - B(T - T_B) + \underbrace{\rho\mathrm{SAR} + P_{\mathrm{chip}}^{(\mathrm{density})}}_{\mathrm{ExternalHeatSources}}\left[\frac{\mathrm{W}}{\mathrm{m}^3}\right] \quad (1)$$

where the expression on the left is the temperature increase per unit time multiplied by the thermal capacitance per unit volume (given as the product of the specific heat of that specific tissue $(C[\mathrm{J}/(\mathrm{kg}\cdot^\circ\mathrm{C})])$ and density of that tissue $(\rho[\mathrm{kg}/\mathrm{m}^3])$). The terms on the right represent the different ways of heat accumulation or removal from the tissue, where

$\nabla\cdot(K\nabla T)$ thermal spatial diffusion term leading to heat transfer through conduction $(K[\mathrm{J}/\mathrm{m}\cdot\mathrm{s}\cdot^\circ\mathrm{C}])$;

A tissue-specific internal metabolic heat production $(\mathrm{J}/(\mathrm{m}^3\cdot\mathrm{s}))$;

TABLE I
THERMAL PARAMETERS OF THE HEAD MODEL TISSUES UNDER NATURAL STEADY STATE CONDITIONS AND MATERIAL COMPOSITION OF THE HEATER PROBE AND IMPLANTED CHIP

Tissue	C J/(kg $\cdot^\circ$ C)	K J/(m $\cdot$ s $\cdot^\circ$ C)	B_0 J/(m^3 $\cdot$ s $\cdot^\circ$ C)	A_0 J/(m^3 $\cdot$ s)
Air (Internal)	1300	0.030	0	0
Aqueous Humor	3997	0.594	0	0
Blood	3840	0.530	0	0
Bone cortical	1300	0.400	3400	610
Bone cancellous	1300	0.400	3300	590
Bone marrow	2700	0.220	32000	5700
Brain Grey matter	3700	0.570	35000	10000
Brain white matter	3600	0.500	35000	10000
Cartillage	3400	0.450	9100	1000
Cornea	4178	0.580	0	0
Cerebro Spinal Fluid	4200	0.620	0	0
Eye's ciliary muscle	4178	0.580	0	0
Fat	2500	0.250	520	180
Lens	3000	0.400	0	0
Muscle	3600	0.500	2700	690
Mucous membrane	3300	0.430	9000	1600
Retina	3680	0.565	35000	10000
Skin	3500	0.420	9100	1000
Vitreous Humor	3997	0.578	0	0
Composition of IMPLANTED HEATER and its thermal properties				
Te¤on	1172	0.200	0	0
Ceramic	1025	29.00	0	0
Copper	380	60.00	0	0
Composition of IMPLANTED CHIP and its thermal properties				
Composite material	700	60.00	0	0
Insulation	880	30.00	0	0

B tissue-specific capillary blood perfusion coefficient ($\mathrm{J}/(\mathrm{m}^3 \cdot \mathrm{s} \cdot^\circ \mathrm{C})$, leading to heat transfer proportional to difference in tissue temperature (T) and blood temperature (T_B), and the external heat sources $\rho\mathrm{SAR}$ due to induced EM power deposition and $P_{\mathrm{chip}}^{\mathrm{density}}$ due to implanted chip power dissipation.

Heat exchange at the tissue interface with the surrounding environment is modeled by imposing the continuity of heat flow perpendicular to the skin surface as the boundary condition and is expressed as

$$K\frac{\partial T}{\partial n}(x,y,z) = -H_a(T_{(x,y,z)} - T_a)\ \left[\frac{\mathrm{W}}{\mathrm{m}^2}\right] \tag{2}$$

where n is the normal to the skin surface and the right hand expression models the heat losses from surface of the skin due to convection and radiation which are proportional to the difference between the skin temperature $(T_{(x,y,z)})$ and external environment temperature (T_a assumed constant at 24 °C), H_a is the convection coefficient for heat exchange with the external temperature. Heat losses due to sweating are not considered in this study.

Thermoregulatory mechanisms impart the capability to the human body to regulate the temperature at an almost constant value of approximately 37 °C at its core. Owing to the nature of application for the thermal problem in the present work, thermoregulatory effects are considered to influence only two physiological parameters in (1). The tissue-specific basal metabolic rate (A) and blood perfusion coefficient (B) are modeled to be temperature dependent. Thermal dependence of basal metabolic rate is expressed as [25]

$$A(x,y,z,T) = A_0(x,y,z,T)(1.1)^{(T(x,y,z)-T_0(x,y,z))} \tag{3}$$

where T_0 is the basal temperature and A_0 is the basal metabolic rate at cell (x,y,z). The regulatory mechanism affecting the internal tissue blood perfusion coefficient is dependent on the local tissue temperature and can be expressed as [25]

$$B(x,y,z,T) = B_0 \text{ if } T(x,y,z) \le 39^\circ\mathrm{C} \tag{4}$$

$$B(x,y,z,T) = B_0[1 + S_B(T(x,y,z) - 39)] \quad \text{if } 39^\circ\mathrm{C} < T(x,y,z) < 44^\circ\mathrm{C} \tag{5}$$

$$B(x,y,z,T) = B_0(1 + 5S_B) \text{ if } T(x,y,z) > 44^\circ\mathrm{C}. \tag{6}$$

Lastly, thermoregulation in the skin due to vasodilatation is considered by regulating the skin blood flow according to

$$B(x,y,z,T) = [B_0 + F_{sb}\overline{\Delta T_s}] \cdot 2^{((T(x,y,z)-T_0(x,y,z))/6)} \tag{7}$$

where $\overline{\Delta T_s}$ is the average skin temperature increase and F_{sb} is the weight associated with it. The temperature of blood is assumed to be constant at 37 °C and the external environment temperature is fixed at 24°C. S_B is assumed to have a value of 0.8 $^\circ\mathrm{C}^{-1}$ [25] and H_a is assumed to be 10.5 $\mathrm{W}/(\mathrm{m}^2 \cdot^\circ \mathrm{C})$ [26]. It should be noted that this value of H_a is used for both the skin-air and cornea-air interfaces in this work. The value of H_a suggested for the cornea-air interface is 20 $\mathrm{W}/(\mathrm{m}^2 \cdot^\circ \mathrm{C})$ [27]. Though it is not explicitly reported here, simulations have been performed for different values of H_a and the variation in temperature rise on the tissues due to the source of heat (implanted chip power dissipation) was observed to be negligible and hence a constant value of $H_a = 10.5\,\mathrm{W}/(\mathrm{m}^2 \cdot^\circ \mathrm{C})$ has been used for all the simulations in this study. The thermoregulatory influence of sweating is neglected. The thermal parameters for all the tissues in the head model have been directly obtained from either [12] or [25] and are reported in Table I. Thermal parameters of the

choroid are determined on the basis of its physiological functions. Since it is highly vascularized, it is modeled with the dielectric and thermal properties as well as mass density of blood. However, it should be noted that in all the thermal simulations considered, choroidal temperature is not fixed at blood temperature but is allowed to evolve in accordance with the bio-heat equation. Also, the cooling influence of the choroid on the retina is accounted for as mentioned in [12].

As outlined and implemented in [25], (1) and (2) were spatially and temporally discretized to realize an explicit FDTD formulation of the bio-heat equation in the computational domain comprising of the 3-D head-eye model. As a first step, it was necessary to determine the natural steady-state thermal distribution in the head-eye model in the absence of any external heat sources. This basal temperature distribution was then used as the starting point for all thermal simulations involving the operation of the retinal prosthesis.

In Section IV, a validation of the thermal method and model is performed by comparing the simulated results with actual experimental observations in the eyes of dogs. It should be noted that human thermal parameters as mentioned above are used for this validation purpose even though they may not correspond exactly with thermal parameters for dogs.

IV. Thermal Model Validation

Experiments have been performed [28] to investigate the thermal effects of power dissipation from implanted electronics on the vitreous cavity and retina in the eyes of dogs. The main objectives of these studies were to determine the thermal conditions harmful to the retina and aid in the development of an implantable intraocular electronic retinal prosthesis. Two different types of tests were carried out. In protocol 1, a heater probe, each time dissipating a different amount of power was positioned at different points of the retina to observe immediate as well as chronic (four weeks later) thermal damage inflicted. In protocol 2, a heater dissipating 500 mW of power was mechanically held in the vitreous cavity for 2 h. These experiments were carried out on dogs due to the similarity between the eyes of dogs and those of humans. The heater utilized in the experiments was a custom made probe which measured approximately $1.4 \times 1.4 \times 1.0$ mm. The teflon insulation of the probe enclosed a 240 Ω resistor to generate heat. The insulation also included a thermocouple to measure temperature increase right next to the heater. Another thermocouple was positioned in the vitreous cavity to measure temperature increase in the fluid environment.

Due to numerical and physical constraints (inability of the head model to register damage), in this work, only protocol 2 of the experimental study mentioned above was implemented and investigated. The heater was modeled as a $1.5 \times 1.5 \times 1.0$ mm ceramic material connected to a copper wire. Since in the experimental study a teflon insulation was used around the heater resistor, in the model a 1-mm-thick teflon coating insulated the wire and the heater probe from the vitreous cavity. The heater assembly was inserted from the side of the eyeball and the probe was positioned in the center of the vitreous cavity. The relative size of the head model used and placement of the heater is shown in a cross-sectional slice in Fig. 3. As mentioned before, in the thermal simulation the choroidal temperature was not fixed at

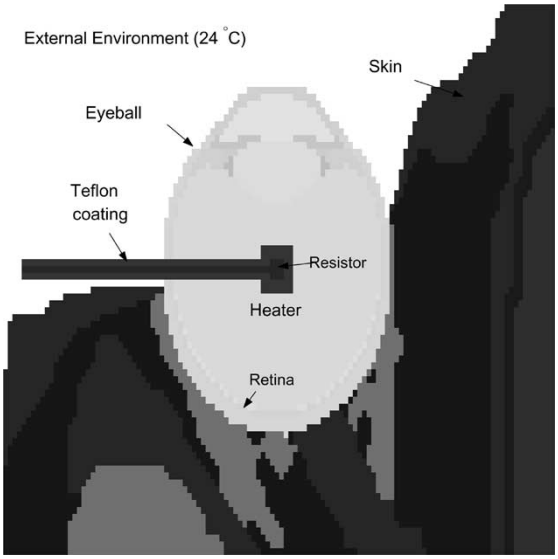

Fig. 3. Cross section of the head model.

T_B but allowed to evolve naturally and the heater was allowed to dissipate 500 mW uniformly for 1 h of simulated physical time. Temperature increase above the basal distribution at several points in the model was recorded and it was observed that thermal elevation reached a steady state within 60 min of physical time.

In the experimental study, five breeds of dogs were subjected to protocol 2 for 2 h and temperature increase in the vitreous cavity and on the heater recorded at discrete intervals of time. Approximately, an average of 6 °C to 8 °C temperature increase was observed in the vitreous cavity, 2°C to 3 °C on the retina and about 50 °C to 60 °C increase was registered on the thermocouple placed on the heater. Histological samples of the eye taken (acutely as well as after four weeks) showed no retinal damage. It was also observed that, despite the high temperature at the heater, the temperature increase in the vitreous cavity remained within several degrees and it was concluded that the fluid environment (vitreous humor) acted as an ideal heat sink in dissipating the heat generated by the heater probe (or implanted electronics).

Numerically, after 60 min of implementing protocol 2, the temperature increase obtained in the vitreous cavity, retinal tissue and at the heater showed good agreement with the experimentally measured values. The mid-vitreous region registered a temperature increase of approximately 8 °C to 9 °C while the temperature of the retinal tissue increased by 4 °C to 6 °C. Temperature at the heater also increased by 60 °C. In the numerical model, increases in temperature of 0.07 °C in white matter of the brain, 0.18 °C in the sinuses of the forehead, 6.03 °C on the cornea, and 1.07 °C on the skin of cheek were observed after 60 min of the mid-vitreous heater dissipating 500 mW.

The experimental study did not outline the precise locations of the thermocouple while recording the temperature increase at the retina and in the mid vitreous. Computationally, this led to some uncertainty in selecting specific points (in the mid-vitreous and on the retina) at which to record the temperature increase. The slight difference in experimentally measured and numerically obtained thermal elevation results is attributed to

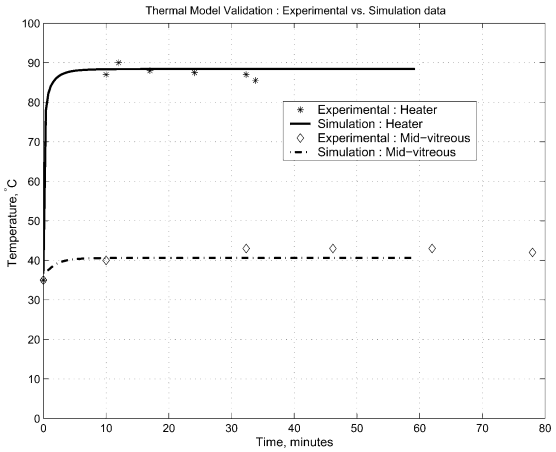

Fig. 4. Experimentally observed versus numerically obtained data.

this variation in the selection of specific points in the model. Fig. 4 shows the experimental and simulated temperature data monitored at definite intervals for a point next to the heater and in the mid-vitreous. The close agreement observed between the experimental and measured data indicates that the current model and simulation method employed are sufficiently reliable for estimating the thermal elevation in biological tissues due to power dissipated by prosthetic implants.

Since this was a validation of the thermal model and method used, it was of interest to study the cooling effect of the thermoregulatory mechanisms. Hence, two cases of numerical implementation of the bio-heat equation were considered. In the first case, the thermoregulatory mechanisms (time dependency of B_0 and A_0 and vasodilatation) were included in the bio-heat equation while in the second case thermoregulatory mechanisms were neglected. Several tissue points were monitored and it was observed that the difference in temperature rise between the two cases was of the order of a few hundredths of a degree despite the fact that the actual temperature of that tissue rose by a few degrees in each case. Thus, in all the simulations with implanted chips, the thermoregulatory effects were neglected.

V. Numerical Results for Thermal Elevation Due to Operation of the Wireless Telemetry Link and Implanted Chip

A. SAR Results

Power absorption in the head and eye tissues due to the wireless link was computed by modeling a 2-A current at 10 MHz excited in a single turn circular coil of approximately 37-mm diameter positioned 20 mm away from the cornea. Peak 1-g SAR value was evaluated and observed to be $\mathrm{SAR}_{1g} = 0.021$ [W/kg]. Since at these currently estimated operating power and current levels, the SAR values for the inductive communication link do not exceed the IEEE safety limits for power absorption [22], the contribution of SAR to the final temperature elevation would be negligible as compared to the rise in temperature due to power dissipation in the implanted chip. Therefore, the power dissipation of the implanted chip alone has been considered as an external heat source in the thermal simulations.

B. Thermal Elevation Results

In order to compute the thermal elevation in the head model due to implanted electronics, it was necessary to first obtain the natural basal temperature distribution in the absence of any external heat sources. The basal temperature distribution was obtained for the larger portion of the head model shown in Fig. 2 (as noted in Section II) with no external heat sources and the external environment temperature being fixed at 24 °C. A portion of this model was extracted and the implant was modeled with the dimensional and material properties of an electronic chip. This implanted chip was modeled to have a composite thermal conductivity (K) of 60 $[\mathrm{J/m \cdot s \cdot^{\circ} C}]$ and encapsulated in a 0.5-mm-thick layer of insulation $(K = 30[\mathrm{J/m \cdot s \cdot^{\circ} C}])$. Several thermal simulations were performed with the chip modeled with different sizes, placed at different locations (in the eyeball) and also dissipating different amounts of power in order to gain an insight into the best possible configuration (from the point of view of least thermal elevation) for an implant in the eye. In Sections V-B1–V-B3, results obtained for all the different cases considered are presented.

1) Influence of Location of Implant on Tissue Heating: Two locations are being considered for the placement of implanted electronics. In the first case, the lens is removed and the implanted chip is hinged between the ciliary muscles of the eye (referred to as the *anterior* position). The other position under consideration is in the middle of the vitreous cavity parallel to the axis of the eyeball (referred to as the *center* position). The head model used is the same as the one utilized in the thermal validation case. The implanted chip is modeled at both these aforementioned locations and thermal simulations performed to study the variation in temperature increase in different tissues as a function of the implant location.

For both the above cases, the size of the implanted chip was kept constant at $4 \times 4 \times 0.5$ mm (exclusive of the 0.5-mm insulating material) and was allowed to dissipate 12.4 mW (anticipated worst-case power dissipation from an implanted current stimulator chip driving a 16–electrode array positioned on the retina). The power density for each cell $(\mathrm{W/m^3})$ was calculated from the total power dissipated (12.4 mW) and was kept uniform for each cell of the modeled chip throughout its size [12]. Fig. 5(a) and (b) show the temperature increase observed in the different tissues with the implanted chip in anterior and center positions, respectively, allowed to dissipate 12.4 mW for approximately 26 min of simulated physical time.

The maximum temperature increase for both the chip positions is obtained on the surface of the insulating layer. At the specific location monitored in the numerical simulation, it is observed to be about 0.82 °C for both chip positions. As can be expected, due to its proximity to a chip placed in the anterior region, the ciliary muscles for this case heat up by 0.36 °C as compared to 0.19 °C with the chip in the center position. Temperature rise in the vitreous cavity is observed to be 0.26 °C for the chip placed in center while a anterior chip raises its temperature by 0.16 °C. Even though there is no standard accepted threshold for the induction of thermal damage on the retina, it is a very sensitive membrane on which temperature rise is of interest since in an actual prosthesis it is proposed that an electrode

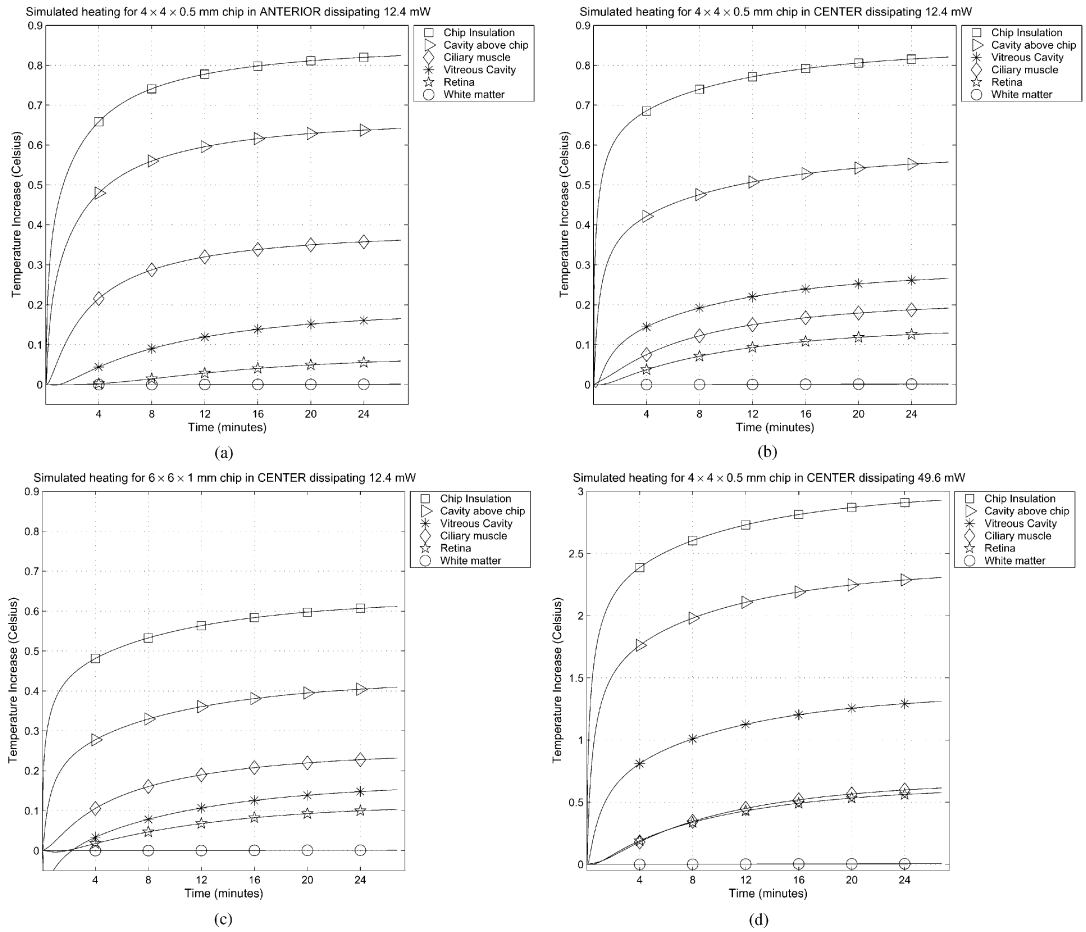

Fig. 5. Simulated heating for different configurations. (a) Anterior positioned 4 × 4 × 0.5 mm chip dissipating 12.4 mW. (b) Center positioned 4 × 4 × 0.5 mm chip dissipating 12.4 mW. (c) Center positioned 6 × 6 × 1 mm chip dissipating 12.4 mW. (d) Center positioned 4 × 4 × 0.5 mm chip dissipating 49.6 mW.

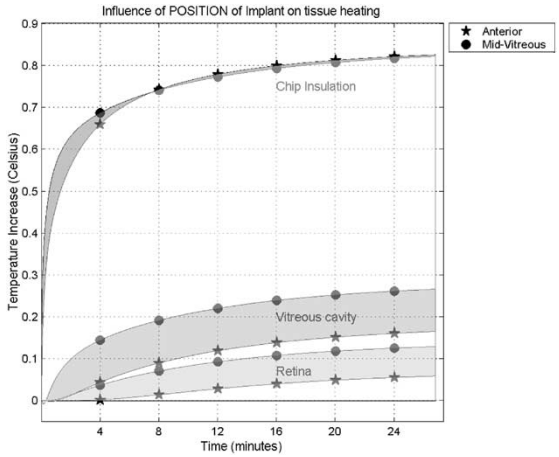

Fig. 6. Simulated thermal rise showing the influence of chip's LOCATION.

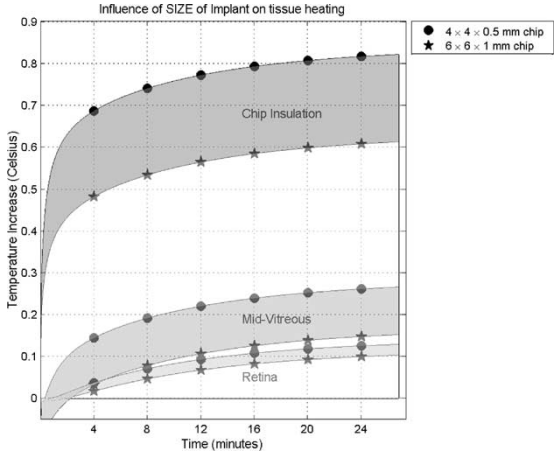

Fig. 7. Simulated thermal rise showing the influence of chip's SIZE.

array will rest on the retina to provide artificial stimulation. An anterior placed chip raises retina's temperature by less than half the amount that a chip placed in the center does (0.05 °C by anterior chip as compared to 0.12 °C by a center chip). Here, also, the vitreous cavity seems to be acting as a heat sink since the rise in temperature of tissues farther from the eye is very small indicating that a miniscule amount of heat flows beyond the eye ball. Fig. 6 graphically compares the temperature increases on the insulator, vitreous cavity and the retina between a anterior placed chip and a center placed chip. It is observed that the anterior position is preferable in order to minimize the temperature rises in the vitreous cavity and on the retina.

2) Influence of SIZE of Implant on Tissue Heating: Besides location, the physical size of the implant is another parameter which can be varied to bring about a reduction in temperature elevation for a given amount of power dissipation. Hence, it is of interest to investigate the effect of *increase* in the implanted chip's size on thermal elevation for a fixed amount of power

TABLE II
SIMULATED TISSUE HEATING OBSERVED DUE TO VARIATION IN IMPLANT'S SIZE, LOCATION AND POWER DISSIPATION LEVEL

	Increase above basal temperature ($\Delta T = T - T_0$) (°C) Observed cases for different size, location and power dissipation level of Implanted chip:				
	Case 1	**Case 2**	**Case 3**	**Case 4**	
Tissue at which thermal rise was monitored	Center $6 \times 6 \times 1$ mm 12.4 mW	Anterior $4 \times 4 \times 0.5$ mm 12.4 mW	Center $4 \times 4 \times 0.5$ mm 12.4 mW	Center $4 \times 4 \times 0.5$ mm 49.6 mW	Ratio $\frac{(\text{Case4})}{(\text{Case3})}$
Insulator around chip	0.61	0.82	0.82	2.92	3.56
Eye's ciliary muscle	0.23	0.36	0.19	0.61	3.21
Cavity just above chip	0.40	0.64	0.55	2.30	4.18
Vitreous cavity	0.15	0.16	0.26	1.31	5.03
Retina	0.10	0.05	0.12	0.57	4.75
White matter of brain	0.001	0.001	0.001	0.005	5.00
Forehead sinuses	0.003	0.003	0.003	0.013	4.33
Skin on forehead	0.002	0.002	0.002	0.010	5.00
Skin of cheek	0.029	0.042	0.026	0.097	3.73

dissipation. Two sizes of the implanted chip are considered: $4 \times 4 \times 0.5$ mm (small) and $6 \times 6 \times 1$ mm (large). In both cases, the chips are placed in center position and allowed to dissipate 12.4 mW of power for 26 min of simulated physical time. Again, the power density is kept uniform for each cell throughout the size of the chip and with both chips dissipating the same power, the power density for each cell of the larger chip is much smaller than that for each cell of the smaller chip. Fig. 5(b) and (c) show the temperature increase observed in the different tissues with the small and large implanted chips in the center position dissipating 12.4 mW of power for 26 min of simulated physical time.

Fig. 7 graphically compares the temperature increase observed on the insulator, in the vitreous cavity and on the retina for both the cases. With the larger chip (less power density), temperature rise decreases on the insulator by 0.20°C, in the vitreous cavity by 0.11 °C, and on the retina by 0.02 °C as compared to temperature rise due to the smaller chip. However, it is observed that thermal elevation in tissues lying toward the anterior portion of the model (toward the external environment like cornea, cilliary muscle, skin *et al.*), is slightly higher due to the larger chip than the smaller chip. The reason for this slight increase may be attributed to the following factors. The larger chip extends out by a few cells in all the directions as compared to the smaller chip. Since blood perfusion in anterior tissues is lesser thus facilitating less natural cooling, temperature increase in this portion is slightly more as compared to that observed for smaller chip, i.e., in the anterior tissues, it is the proximity to the chip which dictates the temperature increase rather than the chip's power density. While in tissues posterior to the chip (retina, muscle), higher blood perfusion facilitates more cooling, and hence the power density of the chip influences the temperature increase (rather than the proximity to the chip). Thus, in the posterior tissues, temperature increase with the larger chip is less than that observed for the smaller chip. Table II reports the simulated heating observed in different tissues after 26 min of simulated physical time for different configurations of the implant.

3) Influence of POWER DISSIPATION of Implant on Tissue Heating: The maximum value of allowable power dissipation in an implant is decided by a fine tradeoff between satisfaction of its functional requirements and prevention of any thermal damage on the surrounding tissues. It is of interest to observe the influence of varying power dissipation levels on corresponding thermal elevation incurred in the head model. In the 16-electrode array design of the retinal prosthesis chip, power dissipation in the implanted chips is not expected to rise above 12.4 mW. To investigate the influence of varying power dissipation, thermal rise is computed with the chip dissipating 12.4 mW in the first case and 49.6 mW in the second case (for the same size chip $4 \times 4 \times 0.15$ mm placed in the center position). Power density is again kept uniform throughout the chip's size. Fig. 5(b) and (d), respectively, show the temperature increase observed in the different tissues with the center placed $4 \times 4 \times 0.15$ mm chip dissipating 12.4 and 49.6 mW for 26 min of simulated physical time.

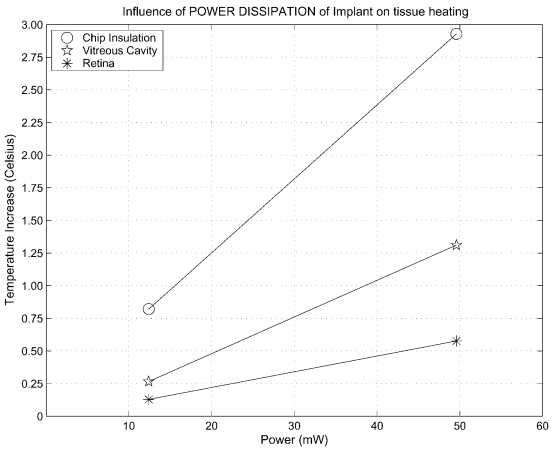

Fig. 8. Simulated thermal rise showing the influence of chip's POWER DISSIPATION.

Fig. 8 graphically compares the temperature increase observed on the insulation, in the vitreous cavity and on the retina for both the cases. From the thermal elevation results as tabulated in Table II, it is observed that increasing the power dissipation by a factor of 4 does not necessarily lead to a rise in the temperature by factor of 4. As reported in Table II, on the insulator, the temperature rose by a factor of 3.57 while in the vitreous cavity and the on the retina temperature increased by 4.93 and 4.47 times, respectively. In the majority of tissues, a temperature rise by a factor of around 3.5 to 5 is observed for a four times increase in the power dissipation in the implant.

VI. CONCLUSION

A detailed numerical investigation of the thermal elevation induced in the head and eye on account of the operation of a

retinal prosthetic system is presented. The retinal prosthetic system considered comprises of an extraocular and an implanted intraocular unit linked together by a wireless telemetry link for power and data communication. The retinal prosthesis is designed to restore a form of vision in the blind by artificially stimulating the retinal cells. Operation of such a prosthetic device causes a rise in the natural steady-state temperature of the eye and surrounding head tissues. In the present work, two aspects of operation of the retinal prosthesis that lead to thermal elevation are considered: EM power deposition due to the operation of the wireless telemetry link and power dissipation in the implanted microchips.

It is noted that the SAR induced due to operation of the considered wireless telemetry link (inductive power and data transfer using coils at 10 MHz) is within the IEEE/ANSI [22] stipulated guidelines.

Several thermal simulations were performed to study the temperature elevation associated with the power dissipation in the implanted chip. When the chip is placed in the anterior position, the temperature increases on the vitreous cavity and retina were less by 0.1 °C and 0.07 °C, respectively, as compared to the case when the chip was located in the center of the vitreous cavity. Also, a larger chip ($6 \times 6 \times 1$ mm as compared to $4 \times 4 \times 0.15$ mm) dissipating the same amount of power reduced the temperature increase on the vitreous cavity and retina by 0.11 °C and 0.02 °C, respectively. A four times rise in the power dissipation in the implant led to a corresponding temperature rise by a factor of 3.5 to 5 depending on the specific tissue.

An investigation of the thermal elevation incurred due to electronic implants in the eye has been performed. The use of a 3-D model instead of the 2-D model employed in [12] facilitated the detailed characterization of the profile of the head and temperature distribution on the chip and eye. Due to excessive computation times, temperature rise on the tissues is monitored for 26 min of physical time, at which time the temperature rise is estimated to be within 5% of the steady-state temperature increase. Future work incorporating the thermal effect of the power dissipation in the stimulating electrode array on the retina can be considered to further characterize the thermal issues associated with the operation of a retinal prosthesis.

REFERENCES

[1] A. Santos, M. S. Humayun, E. de Juan Jr, R. J. Greenberg, M. J. Marsh, and A. H. Milam, "Inner retinal preservation in retinitis pigmentosa: A morphometric analysis," *Arch. Ophthalmol.*, vol. 115, pp. 511–515, 1997.

[2] E. Margalit, M. Maia, J. D. Weiland, R. J. Greenberg, G. Y. Fujii, G. Torres, D. V. Piyathaisere, T. M. O'Hearn, W. Liu, G. Lazzi, G. Dagnelie, D. A. Scribner, E. de Juan Jr, and M. S. Humayun, "Retinal prosthesis for the blind," *Survey of Ophthalmol.*, vol. 47, no. 4, pp. 335–356, 2002.

[3] M. S. Humayun, E. de Juan Jr, J. D. Weiland, G. Dagnelie, S. Katona, R. J. Greenberg, and S. Suzuki, "Pattern electrical stimulation of the human retina," *Vis. Res.*, vol. 39, pp. 2569–2576, 1999.

[4] E. Zrenner, "Will retinal implants restore vision?," *Science*, vol. 295, pp. 1022–1025, Feb. 2002.

[5] W. Liu, M. S. Humayun, E. McGucken, E. de Juan Jr, J. D. Weiland, S. C. DeMarco, and M. Clements, "Multiple unit artificial retina chipset system to benefit the visual impaired," in *Intelligent Systems for the Disabled*, N. Theodorescu, Ed. Boca Raton, FL: CRC Press, 2000, ch. 2.

[6] J. Wyatt and J. F. Rizzo, "Ocular implants for the blind," *IEEE Spectrum*, vol. 33, pp. 47–53, Jan. 1996.

[7] A. Y. Chow, M. T. Pardue, G. A. Peyman, and N. S. Peachey, "Development and application of subretinal semiconductor microphotodiode array," in *Vitreoretinal Surgical Techniques*, F. A Peyman, S. A. Meffert, M. D. Conway, and F. Chou, Eds. London, U.K.: Martin Dunitz, 2001, p. 576.

[8] R. A. Normann, E. M. Maynard, P. J. Rousche, and D. J. Warren, "A neural interface for a cortical vision prosthesis," *Vis. Res.*, vol. 39, no. 15, pp. 2577–2587, 1999.

[9] W. Liu, K. Vichienchom, M. Clements, S. C. DeMarco, C. Hughes, E. McGucken, M. S. Humayun, E. de Juan Jr, J. D. Weiland, and R. J. Greenberg, "A neuro-stimulus chip with telemetry unit for retinal prosthetic device," *IEEE J. Solid-State Circuits*, vol. 35, pp. 1487–1497, Oct. 2000.

[10] S. C. DeMarco, M. Clements, K. Vichienchom, W. Liu, M. Humayun, E. de Juan, J. Weiland, and R. Greenberg, "An epi-retinal visual prosthesis implementation," in *Annu. Conf. BMES*, vol. 1, 1999, p. 475.

[11] E. R. Adair and R. C. Petersen, "Biological effects of radiofrequency/microwave radiation," *IEEE Trans. Microwave Theory Tech.*, vol. 50, pp. 953–962, Mar. 2002.

[12] S. C. DeMarco, G. Lazzi, W. Liu, J. D. Weiland, and M. S. Humayun, "Computed SAR and thermal elevation in a 0.25 mm 2-D model of the humal eye and head in response to an implanted retinal stimulator: Parts 1 and 2," *IEEE Trans. Antennas Propagat.*, vol. 51, pp. 2274–2286, Sept. 2003.

[13] J. Wang and O. Fujiwara, "FDTD computation of temperature rise in the human head for portable telephones," *IEEE Trans. Microwave Theory Tech.*, vol. 47, pp. 1528–1534, Aug. 1999.

[14] P. Bernardi, M. Cavagnaro, S. Pisa, and E. Piuzzi, "Specific absorption rate and temperature increases in the head of a cellular-phone user," *IEEE Trans. Microwave Theory Tech.*, vol. 48, pp. 1118–1126, July 2000.

[15] ——, "SAR distribution and temperature increases in an anatomical model of the human eye exposed to the field radiated by the user antenna in a wireless LAN," *IEEE Trans. Microwave Theory Tech.*, vol. 46, pp. 2074–2082, Dec. 1998.

[16] A. Taflove and M. E. Brodwin, "Computation of the electromagnetic fields and induced temperatures within a model of the microwave-irradiated human eye," *IEEE Trans. Microwave Theory Tech.*, vol. 23, pp. 888–896, Nov. 1975.

[17] A. Hirata, S. I. Matsuyama, and T. Shiozawa, "Temperature rises in the human eye exposed to EM waves in the frequency range 0.6–6 GHz," *IEEE Trans. Electromagn. Compat.*, vol. 42, pp. 386–393, Nov. 2000.

[18] A. Hirata, U. Ushio, and T. Shiozawa, "Formation of hot spots in the human eye for plane wave exposures," in *Asia Pacific Microwave Conf.*, vol. 2, 1999, pp. 477–480.

[19] The National Library of Medicine. (2000) The Visible Human Project. [Online]. Available: http://www.nlm.nih.gov/research/visible/visible_human.html

[20] K. Gosalia, P. Brown, W. Liu, and G. Lazzi, "FDTD investigation of a microwave link for data telemetry in retinal prosthesis applications," in *Proc. Int. Symp. Antennas and Propagation*, vol. 1, 2002, pp. 807–810.

[21] Italian National Research Council. Dielectric Properties of Body Tissue. [Online]. Available: http://safeemf.iroe.fi.cnr.it/tissprop/

[22] *IEEE Standard for Safety Levels With Respect to Human Exposure to Radio Frequency Electromagnetic Fields, 3 kHz to 300 GHz*, IEEE Standard C95.1, 1999.

[23] D. Sullivan, *Electromagnetic Simulation Using the FDTD Method*. New York: IEEE Press, 2000.

[24] G. Lazzi, O. P. Gandhi, and D. Sullivan, "Use of PML absorbing layers for the truncation of the head model in cellular telephone simulations," *IEEE Trans. Microwave Theory Tech.*, vol. 48, pp. 2033–2039, Nov. 2000.

[25] P. Bernardi, M. Cavagnaro, S. Pisa, and E. Piuzzi, "Specific absorption rate and temperature elevation in a subject exposed in the far-field of radio-frequency sources operating in the 10–900 MHz range," *IEEE Trans. Biomed. Eng.*, vol. 50, pp. 295–304, Mar. 2003.

[26] H. N. Kritikos, K. R. Foster, and H. P. Schwan, "Temperature profiles in spheres due to electromagnetic heating," *J. Microwave Power*, vol. 16, no. 3/4, pp. 327–344, 1981.

[27] J. J. W. Lagendijk, "A mathematical model to calculate temperature distributions in human and rabbit eyes during hyperthermic treatment," *Phys., Med., Biol.*, vol. 27, no. 11, pp. 1301–1311, 1982.

[28] D. V. Piyathaisere, E. Margalit, S. J. Chen, J. S. Shyu, S. A. D'Anna, J. D. Weiland, R. R. Grebe, L. Grebe, G. Fujii, S. Y. Kim, R. J. Greenberg, E. de Juan Jr, and M. S. Humayun, "Heat effects on the retina," *Ophthalm. Surg. and Lasers Imaging*, vol. 34, no. 2, pp. 114–120, Mar.–Apr. 2003.

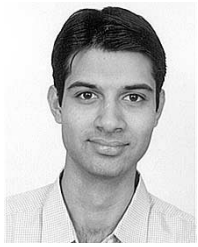

Keyoor Gosalia (S'04) received the B.Eng. degree in electronics from Sardar Patel University, Gujarat, India, in 1999 and the M.S. degree in electrical engineering from North Carolina State University, Raleigh, in 2001, where he is currently working toward the Ph.D. degree in electrical engineering.

His research interests include application of the FDTD method for bioelectromagnetics and novel design techniques for miniature implantable antennas and planar ultra-wideband antenna systems for improving MIMO channel capacity.

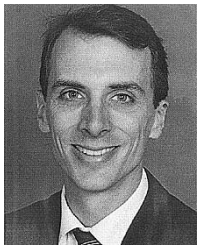

James Weiland (S'92–M'97) received the B.S. degree in 1988, the M.S. degrees in biomedical engineering and electrical engineering in 1993 and 1995, respectively, and the Ph.D. degree in biomedical engineering in 1997, all from the University of Michigan, Ann Arbor.

After four years in industry with Pratt & Whitney Aircraft Engines, he joined the Wilmer Ophthalmological Institute at Johns Hopkins University, Baltimore, MD, in 1997 as a postdoctoral Fellow, and in 1999 was appointed Assistant Professor of Ophthalmology at Johns Hopkins. He joined the Doheny Eye Institute, Los Angeles, CA, in 2001 as part of a larger group of faculty that collectively founded the Doheny Retina Institute. Currently, he is the Director of the Intraocular Retinal Prosthesis Lab at the Doheny Retina Institute, and an Assistant Professor of Ophthalmology at Keck School of Medicine, University of Southern California (USC), Los Angeles, and an Assistant Professor of Biomedical Engineering at USC. His research interests include retinal prostheses, neural prostheses, electrode technology, visual-evoked responses, and implantable electrical systems.

He is a member of the IEEE Engineering in Medicine and Biology Society, the Biomedical Engineering Society, and the Association for Research in Vision and Ophthalmology.

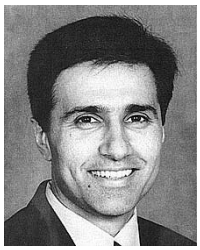

Mark Humayun (M'97) received the Ph.D. degree from Duke University Medical School, Durham, NC, in 1989 and the Ph.D. degree in biomedical engineering from the University of North Carolina, Chapel Hill, in 1993.

He then served a residency in ophthalmology at Duke Eye Center and fellowships at the Retinovascular Center at Johns Hopkins Hospital, Baltimore, MD, and in vitreoretinal surgery at the Johns Hopkins Medical Institution. As Assistant Professor of Ophthalmology at the Johns Hopkins Wilmer Eye Institute from 1995 to 2001, his research focused on microelectronic solutions for severe retinal disease. He joined the Doheny Retina Institute of the Doheny Eye Institute, Los Angeles, in August 2001, where his three appointments include ophthalmology, biomedical engineering, and cell and neurobiology. He is Professor of Ophthalmology at the Keck School of Medicine, University of Southern California, Los Angeles, and Associate Director of Research at the Doheny Retina Institute, where he provides patient care while developing innovative techniques and diagnostics to treat blinding retinal disorders. His quest to find a cure for currently untreatable blinding retinal diseases led him to become one of the primary creators of the intraocular retinal prosthesis that was recently implanted into the first patient in an FDA investigational device study.

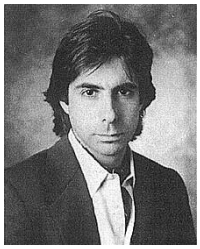

Gianluca Lazzi (S'94–M'95–SM'99) was born in Rome, Italy, in 1970. He received the Dr.Eng. degree in electronics in 1994 from the University of Rome "La Sapienza," Rome, Italy, and the Ph.D. degree in electrical engineering in 1998 from the University of Utah, Salt Lake City.

He has been a Consultant for several companies (1988–1994), Visiting Researcher at the Italian National Board for New Technologies, Energy, and Environment (ENEA) (1994), a Visiting Researcher at the University of Rome "La Sapienza" (1994–1995), and Research Associate (1995–1998) and Research Assistant Professor (1998–1999) at the University of Utah. He is presently an Associate Professor with the Department of Electrical and Computer Engineering, North Carolina State University, Raleigh, after having been an Assistant Professor from 1999 to 2003. He is author or co-author of more than 75 international journal articles or conference presentations on FDTD modeling, dosimetry, and bioelectromagnetics.

Dr. Lazzi received the 2003 ALCOA Foundation Engineering Research Achievement Award, a 2003 NCSU Outstanding Teacher Award, the 2003 NCSU Alumni Outstanding Teacher Award, a 2001 National Science Foundation (NSF) CAREER Award, a 2001 Whitaker Foundation "Biomedical Engineering Grant" for Young Investigators, a 1996 International Union of Radio Science (URSI) "Young Scientist Award," and the 1996 "Curtis Carl Johnson Memorial Award" for the best student paper presented at the eighteenth annual technical meeting of the Bioelectromagnetics Society (BEMS). He is an Associate Editor for the IEEE ANTENNAS AND WIRELESS PROPAGATION LETTERS and the Guest Editor of the Special Issue on Biological Effects and Medical Applications of RF/Microwaves of the IEEE TRANSACTIONS ON MICROWAVE THEORY AND TECHNIQUES (2004). He is listed in *Who's Who in the World*, *Who's Who in America*, *Who's Who in Science and Engineering*, the *Dictionary of International Biographies*, and *2000 Outstanding Scientists of the 20th Century*.